 Preprint from Nuclear Instruments and Methods in Physics Research B 332 (2014) 143–147

Emission channeling studies on transition-metal doped GaN and ZnO: Cation versus anion substitution

L.M.C. Pereira [a], *, U. Wahl [b], J.G. Correia [b], L.M. Amorim [a], D.J. Silva [c], S. Decoster [a], M.R. da Silva [d], K. Temst [a], A. Vantomme [a]

[a] *KU Leuven, Instituut voor Kern- en Stralingsfysica, 3001 Leuven, Belgium*
[b] *Centro de Ciências e Tecnologias Nucleares, Instituto Superior Técnico, Universidade de Lisboa, 2695-066 Bobadela, Portugal*
[c] *IFIMUP and IN-Institute of Nanoscience and Nanotechnology, Departamento de Física e Astronomia da Faculdade de Ciências da Universidade do Porto, 4169-007 Porto, Portugal*
[d] *Centro de Física Nuclear da Universidade de Lisboa, 1649-003 Lisboa, Portugal*

* Corresponding author, email: lino.pereira@fys.kuleuven.be

DOI: http://dx.doi.org/10.1016/j.nimb.2014.02.048

Abstract

The magnetic and electric properties of impurities in semiconductors are strongly dependent on the lattice sites which they occupy. While the majority site can often be predicted based on chemical similarities with the host elements and is usually simple to confirm experimentally, minority sites are far more complicated to predict, detect and identify. We have carried out extensive β^- emission channeling studies on the lattice location of transition metal impurities in wide-gap dilute magnetic semiconductors, namely Co and Mn in GaN and ZnO, making use of radioactive ^{61}Co and ^{56}Mn implanted at the ISOLDE facility at CERN. In addition to the majority occupation of cation (Ga, Zn) sites, we located significant fractions (of the order of 20%) of the Co and Mn impurities in anion (N, O) sites, which are virtually unaffected by thermal annealing up to 900 °C. Here, we present the β^- emission channeling experiments on ^{61}Co-implanted GaN. We discuss these results in the context of our recent reports of minority anion substitution in Mn-implanted GaN Pereira et al. (2012) [19] and Mn/Co-implanted ZnO Pereira et al. (2011) [20], particularly in terms of the advantages of the emission channeling technique in such cases of multi-site occupancy.

1. Introduction

In a dilute magnetic semiconductor (DMS), magnetic atoms (or impurities) are introduced in an otherwise non-magnetic semiconductor. The co-existence of ferromagnetism and semiconducting behavior in some DMS materials has generated fundamental new physics and enabled the study of phenomena of interest for spintronics [1].

For a given impurity-host combination, the magnetic behavior of a DMS material is strongly dependent on the lattice sites occupied by the magnetic impurities. The canonical example is Mn-doped GaAs, where Mn can occupy both Ga-substitutional and tetrahedral interstitial sites [2,3]. Whereas substitutional Mn provides both the localized magnetic moment and the itinerant hole that mediates the magnetic coupling, interstitial Mn acts as a compensating defect, both electrically and magnetically [4]. In oxide and nitride DMS systems, such as Mn, Fe or Co doped GaN and ZnO, it is generally accepted that the transition metal impurities occupy only cation-substitutional sites, i.e. substitute Ga in GaN and Zn in ZnO, as expected from the chemical similarities. This has been observed experimentally, mostly based on X-ray absorption fine structure (XAFS) but also on conventional ion channeling, and appears to be independent of the doping method, i.e. either during growth (e.g. Refs. [5–14]) or by ion implantation (e.g. Refs. [15–18]). However, using the emission channeling (EC) technique, we have recently located significant fractions of implanted Mn impurities in N (anion) sites in GaN [19]. Similarly, we have also reported the minority anion (O) substitution by Co and Mn impurities in ZnO [20].

Here, we present β^- emission channeling experiments on the lattice location of implanted transition metals in GaN and ZnO. We report β^- emission channeling experiments on implanted Co in GaN and, together with our previous reports on implanted Co in ZnO [20] as well as Fe and Mn in GaN and ZnO [19–22], we discuss the technique's advantages in such cases of multi-site occupancy.

2. Experiment

2.1. Emission channeling technique

The emission channeling (EC) technique probes the lattice location of impurities in single crystals, making use of the charged particles emitted by a radioactive isotope of the impurity element under study [23]. The screened Coulomb potential of atomic rows and planes determines the anisotropic scattering of the particles emitted isotropically during the radioactive decay. Along low-index directions of single crystals, this anisotropic scattering results in well defined channeling or blocking effects. Because these effects strongly depend on the initial position of the emitted particles, they result in emission patterns which are characteristic of the lattice site(s) occupied by the probe atoms. Angular-dependent emission patterns are recorded along various crystallographic axes using a position-and energy-sensitive detection system similar to that described in Ref. [24]. The theoretical emission patterns for probes occupying possible lattice sites are calculated using the manybeam formalism for electron channeling in single crystals [23]. Quantitative lattice location is provided by fitting the experimental patterns with theoretical ones using the two-dimensional fit procedure outlined in Ref. [24]. Corrections for backscattered electrons that reach the detector were implemented by subtracting an isotropic background from every pattern. This backscattered electron contribution is estimated based on Geant4 [25,26] simulations of electron scattering, taking into account the elemental composition and geometry of the sample, sample holder and vacuum chamber.

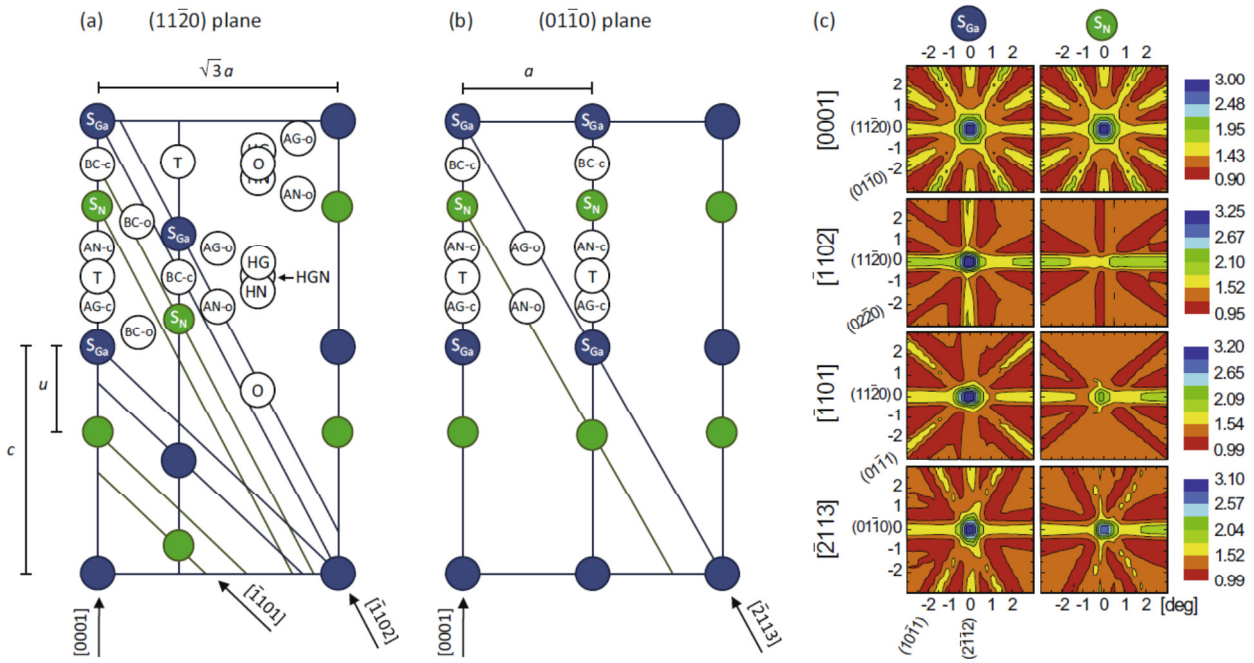

Fig. 1. The (11–20) (a) and (11–10) (b) planes of the GaN wurtzite lattice, showing the substitutional Ga (S_{Ga}) and N (SN) sites as well as the following interstitial sites: bond center BC, antibonding Ga (AG) and antibonding N (AN), octahedral (O), tetrahedral (T) and hexagonal (HG and HN). ''-c'' denotes sites along the *c*-axis and ''-o'' along the basal directions, i.e. off the *c*-axis. Along the [–1101] and [–1102], [–2113] directions, the rows of Ga and N atoms are indicated. In panels (a) and (b), *a*, *c* and *u* indicate the lattice constants and bond length parameter of the wurtzite structure, respectively. (c) Simulated channeling patterns for 100% of emitter atoms (^{61}Co) on substitutional Ga (S_{Ga}) and N (S_N) sites.

Examples for possible lattice sites of higher symmetry in the GaN wurtzite structure are shown in Fig. 1(a) and (b). In addition to substitutional Ga (cation) and N (anion) sites, the following interstitial sites are shown: bond-centered sites along the *c*-axis and the basal directions (BC-c and BC-o), antibonding sites AG-c, AN-c, AG-o, and AN-o, the hexagonal sites HG and HN [27]. T and O sites, which have been considered previously as possible sites for native Ga and N interstitials [27] are also shown. Theoretical patterns were calculated for probes occupying substitutional Ga (S_{Ga}) and N (S_N) sites with varying root-mean-square (rms) displacements, the main interstitial sites described above and interstitial sites resulting from displacements along the c or the basal directions. The GaN crystallographic parameters and room temperature atomic displacements used in the manybeam simulations can be found in Ref. [32]. Fig. 1(c) shows the theoretical emission patterns along the [0001], [−1101] and [−1102], [−2113] axes for 100% of ^{61}Co atoms on substitutional Ga (S_{Ga}) and N (S_N) sites. Because S_{Ga} and S_N sites, as well as the interstitial sites along the *c*-axis (e.g. BC-c and T), are all equivalent in the lattice projection onto the plane perpendicular to the [0001] direction, the corresponding [0001] emission patterns are not distinguishable [Fig. 1(c)]. The same holds for the interstitial sites along the main interstitial axis parallel to the *c*-axis (e.g. O, HG, HN). In order to unambiguously distinguish the lattice sites in wurtzite crystals, it is thus necessary to measure also along other directions, such as the [−1101] and [−1102], and [−2113] axis. In particular, these three directions separate Ga and N atom rows [Fig. 1(a) and (b)], resulting in emission patterns with distinct anisotropies [Fig. 1(c)] and thus allowing for unambiguous site identification. Moreover, comparing the fit results for as many as four different directions allows us to verify the consistency of the analysis in terms of site identification and occupancy quantification.

2.2. ^{61}Co:GaN experimental details

An epitaxial thin film of wurtzite [0001] GaN grown on sapphire was implanted with the precursor isotope ^{61}Mn with the decay chain ^{61}Mn (0.71 s) → ^{61}Fe (6 min) → ^{61}Co (1.6 h) → ^{61}Ni (stable). The implantations were carried out at the on-line isotope separator facility ISOLDE at CERN, which provides mass-separated beams of radioactive Mn isotopes produced by means of 1.4-GeV proton-induced nuclear fission from uranium carbide UC_2 targets and chemically selective laser ion sources [28]. In order to ensure that the contributions of ^{61}Mn and ^{61}Fe β^- particles to the channeling patterns were negligible, the measurements started only after a waiting period of >30 min. The β^- decays of ^{61}Mn and ^{61}Fe transfer recoil energies of about 475 eV and 103 eV to the ^{61}Fe and ^{61}Co daughters, respectively. This ensures that the ^{61}Co atoms are reimplanted, i.e. that they do not inherit the ^{61}Fe lattice site. The implantation was performed at room temperature, under a tilt angle of 17° with respect to the surface normal in order to minimize ion channeling, with an energy of 50 keV and a fluence of 1.5×10^{13} cm^2, resulting in a peak concentration of 3.5×10^{18} cm^3 at a projected range R_p of 236 Å with a 109 Å straggling, estimated using the SRIM code [29]. The low concentration regime (below 1×10^{19} cm^3, i.e. <0.03%) allows us to study the lattice location of Co free from phase segregation.

Angular-dependent emission yields of the β^- particles emitted during radioactive decay were measured at room temperature, along four crystallographic directions, [0001], [−1101] and [−1102], [−2113], in the as-implanted state and after in situ capless annealing in vacuum (<10^{-5} mbar) at 600 °C and 900 °C. These patterns were recorded using a position-and energy-sensitive detection system similar to that described in Ref. [30]. Given the relatively short half-life of ^{61}Co, this system was installed on-line and upgraded with self-triggering readout chips for the Si pad detectors, enabling measurements during and/or immediately after implantation with count rates of up to several kHz [31].

3. Results and discussion

For all four measured directions, the calculated S_{Ga} patterns gave by far the best agreement, showing that the majority of the probe atoms occupy S_{Ga} sites, as expected. The fitting routine was then allowed to include, in addition to S_{Ga}, an additional lattice site, for which all simulated sites were considered. Consistently for all measured directions, the S_{Ga} + S_N double occupancy gave the best fit compared to all other combinations, and considerably improved the S_{Ga} single-site fit, with up to 13% lower reduced χ^2. Fig. 2(a) shows the reduced χ^2 of the fit as the non-S_{Ga} site is moved along the *c*-axis between two neighboring S_{Ga} sites (the [0001] direction is not included since it does not distinguish sites along the *c*-axis). Consistently for all three directions, the best fits are centered at the S_N site. The sensitivity of the fit (in terms of magnitude and ''width'' of the improvement in χ^2) is correlated with the spatial separation between Ga and N rows along the channeling axis [Fig. 2(b), right], being most pronounced for

the [−2113] direction. For comparison, Fig. 2(b) shows an equivalent χ^2 plot for ^{59}Fe in GaN, obtained by analyzing the data of Ref. [21] using new simulations which include the same lattice sites as in the case of ^{61}Co. No discernible decrease in χ^2 is observed around the S_N site. Instead, the data indicate that a fraction of the ^{59}Fe impurities occupy S_{Ga} sites which are displaced from the ideal S_{Ga} position by ~0.2 Å (consistent with the analysis in Ref. [21]), which indicates the presence of neighboring defects such as N vacancies.

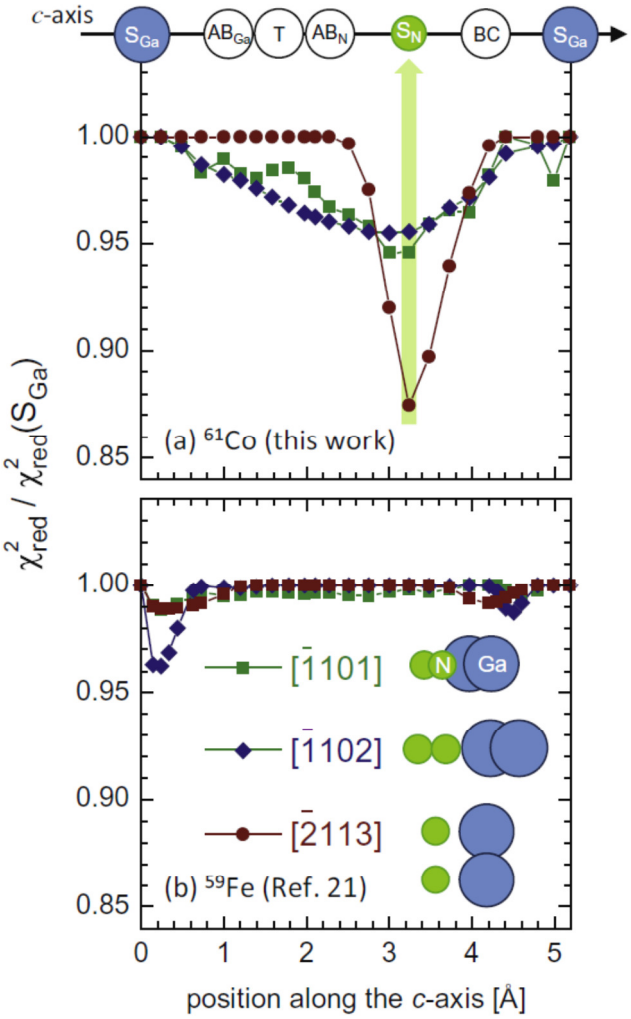

Fig. 2. Reduced χ^2 of the fits to the experimental emission yields in the vicinity of the [−1101] and [−1102], [−2113] directions (following 600 °C annealing), for (a) ^{61}Co (this work) and (b) ^{59}Fe (Ref. [21]). Each data point corresponds to the best fit obtained using two given sites, with the corresponding two fractions as free parameters. The site pairs are composed of S_{Ga} plus the corresponding sites along the *c*-axis (depicted above the plot): the S_N and the T sites, the BC and AB sites along the c-axis and a number of intermediate positions. The *x*-axis corresponds to the position (along the *c*-axis) of the non-S_{Ga} site used in each fit. The reduced χ^2 (*y*-axis) of these two-site fits are normalized to that of the one-site (S_{Ga}) fit. The non-equivalent rows of Ga and N atoms, projected on the plane perpendicular to each of the axes, are also shown [(b), right]. Note that the separation between Ga and N rows is maximized along [−2113] axis.

As an example of the good match between experiment and simulated patterns, Fig. 3 compares the normalized experimental β^- emission yields following annealing at 600 °C, along the four measured directions [(a)–(d)] with the best fits of theoretical patterns [(e)–(h)]. The best fit is obtained for 84% of the ^{61}Co atoms on S_{Ga} (Co_{Ga}) and 14% on S_N sites (Co_N). Introducing a third site yields only insignificant fit improvements. Possible fractions in other sites are estimated to be below 5%. Fig. 4 shows the fractions of ^{61}Co probes in S_{Ga} and S_N sites as a function of

annealing temperature. Within the experimental error, the Co_N fraction remains constant around 15%, up to the highest annealing temperature of 900 °C.

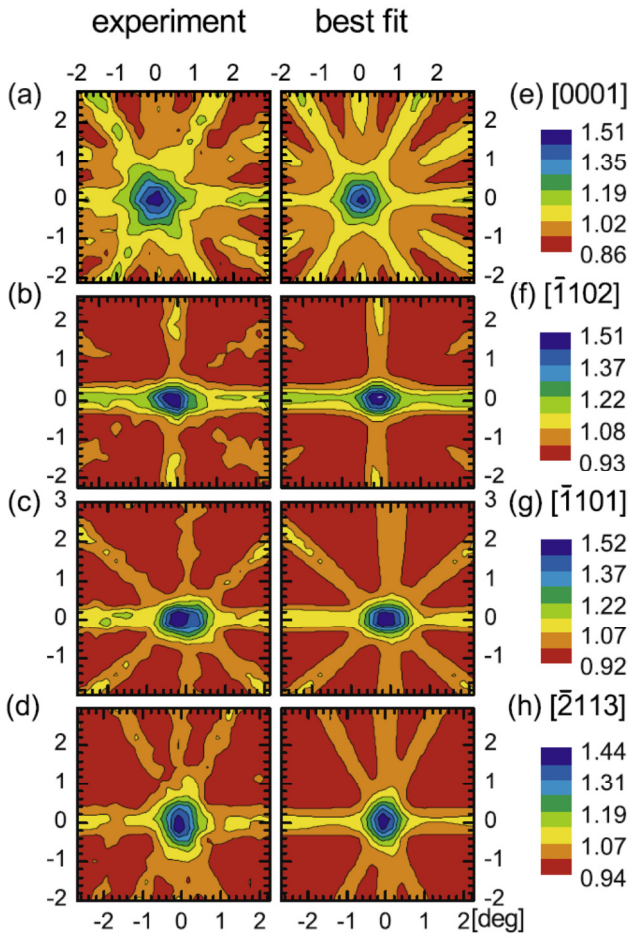

Fig. 3. (a)–(d) Normalized experimental ^{61}Co β^- emission channeling patterns in the vicinity of the [0001], [−1101] and [−1102], [−2113] directions following annealing at 600 °C. (e)–(h) Corresponding best fits with 84% and 14% of the ^{61}Co atoms on S_{Ga} and S_N sites, respectively.

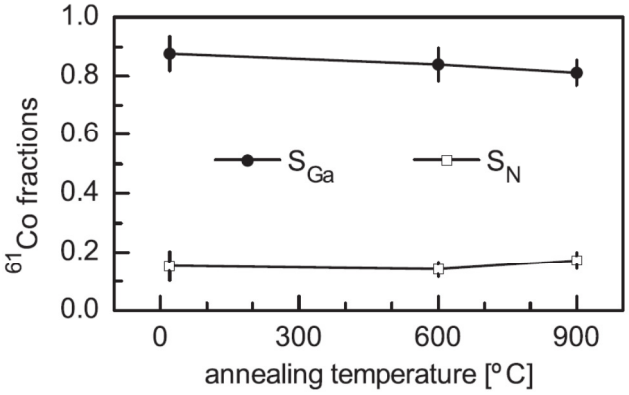

Fig. 4. Fractions of ^{61}Co impurities on S_{Ga} and S_N sites following each annealing step.

The observed anion substitution by transition metal impurities in wurtzite GaN and ZnO is remarkably surprising. No such anion substitutional fractions were detected in previous studies based on XAFS and conventional ion-channeling, for impurities incorporated either during growth (e.g. Refs. [5–14]) or by ion implantation (e.g. Refs. [15–18]). The only report on anion substitution detected by XAFS is for Mn-doped zincblende GaN grown by molecular beam epitaxy (MBE) in N-poor conditions [33]. We note however that in Ref. [33] XAFS was able to detect the anion substitution because the corresponding fraction was remarkably high (75%). This raises an important question of how small the anion-substitutional fraction can be and still be detected by XAFS. Since identifying a minority site in cases of double occupancy is in general extremely challenging for XAFS techniques (which rely on complex multiparameter fitting using calculated model structures), one may ask whether minority anion substitution may have so far escaped detection.

The non-equilibrium nature of ion implantation may play a favorable role on the observed anion substitution, since the high concentration of anion vacancies created upon implantation is likely to facilitate impurity incorporation in anion sites. However, this does not explain why, under very similar experimental conditions, anion substitution does not occur for implanted Fe, both in GaN [21] and ZnO [22]. Just as Mn and Co, Fe is a 3*d* transition metal, with a similar atomic mass and, therefore, similar incorporation kinetics and defect creation. In Refs. [19,20], we have discussed potential mechanisms and implications of anion substitution in dilute magnetic semiconductors. In a wider context of semiconductor doping, where minority-site occupancy is often detrimental to the desired functionality, these findings demonstrate the advantages of emission channeling as a lattice location technique. Since it makes use of 2-dimensional emission patterns, measured using position sensitive detectors, which are directly compared to numerical simulations, it provides unambiguous, quantitative, multi-site lattice location (for site fractions in the % range). This implementation of electron channeling demonstrates how measuring the full angular dependence, and numerically fitting the spectra with accurate simulations, greatly enhances the capabilities of channeling techniques, particularly in comparison to conventional implementations of ion-channeling techniques (Rutherford backscattering spectrometry and particle induced X-ray emission), for which only 1-dimensional angular scans are typically used. In addition, by relying on the particles emitted upon decay of radioactive probes, the emission channeling technique is extremely sensitive in the sense that it requires only a small number of impurities, down to 10^{10} atoms (i.e. several orders of magnitude lower than conventional channeling techniques), making it particularly suited to study very dilute systems.

4. Conclusions

We have experimentally determined the lattice location of implanted Co in wurtzite GaN in the low concentration regime (below 3.5×10^{18} cm^3, i.e. <0.015%). In addition to the majority on substitutional cation (Ga) sites, we located a significant fraction of the Co atoms (~15%) on substitutional anion (N) sites, which was virtually unaffected by thermal annealing up to 900 °C. Together with our previous reports of anion substitution by Mn in GaN and Co/Mn in ZnO, these findings illustrate the advantages of emission channeling in terms of sensitivity and multi-site lattice location capabilities.

Acknowledgments

This work was supported by the Portuguese Foundation for Science and Technology (CERN/FP/123585/2011, SFRH/BD/35761/ 2007), the European Union Seventh Framework through ENSAR (European Nuclear Science and Applications Research, Contract No. 262010) and SPIRIT (Support of Public and Industrial Research Using Ion Beam Technology, Contract No. 227012), the Fund for Scientific Research-Flanders, and KU Leuven Projects No. GOA/ 2009/006 and GOA/2014/007.

References

[1] T. Dietl, Nat. Mater. 9 (2010) 965.
[2] L.M.C. Pereira, U. Wahl, S. Decoster, J.G. Correia, M.R. da Silva, A. Vantomme, J.P. Araújo, Appl. Phys. Lett. 98 (2011) 201905.
[3] L.M.C. Pereira, U. Wahl, S. Decoster, J.G. Correia, L.M. Amorim, M.R. da Silva, J.P. Araujo, A. Vantomme, Phys. Rev. B 86 (2012) 125206.

[4] T. Jungwirth, K.Y. Wang, J. Masek, K.W. Edmonds, J. Konig, J. Sinova, M. Polini, N.A. Goncharuk, A.H. MacDonald, M. Sawicki, A.W. Rushforth, R.P. Campion, L.X. Zhao, C.T. Foxon, B.L. Gallagher, Phys. Rev. B 72 (16) (2005) 165204.
[5] T. Shi, S. Zhu, Z. Sun, S. Wei, W. Liu, Appl. Phys. Lett. 90 (2007) 102108.
[6] Z. Sun, W. Yan, G. Zhang, H. Oyanagi, Z. Wu, Q. Liu, W. Wu, T. Shi, Z. Pan, P. Xu, S. Wei, Phys. Rev. B 77 (2008) 245208.
[7] N. Farley, K. Edmonds, A. Freeman, G. van der Laan, C. Staddon, D. Gregory, B. Gallagher, New J. Phys. 10 (2008) 055012.
[8] J.C. Pivin, G. Socol, I. Mihailescu, P. Berthet, F. Singh, M.K. Patel, L. Vincent, Thin Solid Films 517 (2008) 916.
[9] A. Bonanni, M. Sawicki, T. Devillers, W. Stefanowicz, B. Faina, T. Li, T.E. Winkler, D. Sztenkiel, A. Navarro-Quezada, M. Rovezzi, R. Jakiela, A. Grois, M. Wegscheider, W. Jantsch, J. Suffczynski, F. D'Acapito, A. Meingast, G. Kothleitner, T. Dietl, Phys. Rev. B 84 (2011) 035206.
[10] O. Sancho-Juan, O. Martinez-Criado, A. Cantarero, N. Garro, M. Salome, J. Susini, D. Olguin, S. Dhar, K. Ploog, Phys. Rev. B 83 (2011) 172103.
[11] W. Stefanowicz, D. Sztenkiel, B. Faina, A. Grois, M. Rovezzi, T. Devillers, F. d'Acapito, A. Navarro-Quezada, T. Li, R. Jakiela, M. Sawicki, T. Dietl, A. Bonanni, Phys. Rev. B 81 (2010) 235210.
[12] N. Smolentsev, G. Smolentsev, S. Wei, A.V. Soldatov, Phys. B 406 (2011) 2843.
[13] X. Biquard, O. Proux, J. Cibert, D. Ferrand, H. Mariette, R. Giraud, B. Barbara, J. Supercond. 16 (2003) 127.
[14] S. Kuroda, S. Marcet, E. Bellet-Amalric, J. Cibert, H. Mariette, S. Yamamoto, T. Sakai, T. Ohshima, H. Itoh, Phys. Status Solidi A-Appl. Mater. 203 (2006) 1724.
[15] A. Singh, R. Kumar, P. Thakur, N. Brookes, K. Chae, W. Choi, J. Phys.: Condens. Matter 21 (2009) 185005.
[16] J.A. Sans, G. Martinez-Criado, J. Susini, R. Sanz, J. Jensen, I. Minguez, M. Hernandez-Velez, A. Labrador, P. Carpentier, J. Appl. Phys. 107 (2010) 023507.
[17] J. Baik, S. Kim, Y. Koo, T. Kang, J. Lee, Electrochem. Solid State Lett. 7 (2004)
[18] C. Liu, E. Alves, A. Ramos, M. da Silva, J. Soares, T. Matsutani, M. Kiuchi, Nucl. Instr. Meth. Phys. Res. Sect. B 191 (2002) 544.
[19] L.M.C. Pereira, U. Wahl, J.G. Correia, S. Decoster, L.M. Amorim, M.R. da Silva, J.P. Araujo, A. Vantomme, Phys. Rev. B 86 (2012) 195202.
[20] L.M.C. Pereira, U. Wahl, S. Decoster, J.G. Correia, L.M. Amorim, M.R. da Silva, J.P. Araujo, A. Vantomme, Phys. Rev. B 84 (2011) 125204.
[21] U. Wahl, A. Vantomme, G. Langouche, J.G. Correia, L. Peralta, Appl. Phys. Lett. 78 (2001) 3217.
[22] E. Rita, U. Wahl, J. Correia, E. Alves, J. Soares, Appl. Phys. Lett. 85 (21) (2004) 4899.
[23] H. Hofsass, G. Lindner, Phys. Rep. 201 (3) (1991) 121.
[24] U. Wahl, J.G. Correia, S. Cardoso, J.G. Marques, A. Vantomme, G. Langouche, ISOLDE Collaboration, Nucl. Instr. Meth. Phys. Res. B 136 (1998) 744.
[25] S. Agostinelli et al., Nucl. Instr. Meth. Phys. Res. Sect. A 506 (2003) 250.
[26] J. Allison et al., IEEE Trans. Nucl. Sci. 53 (2006) 270.
[27] P. Boguslawski, E.L. Briggs, J. Bernholc, Phys. Rev. B 51 (1995) 17255.
[28] V.N. Fedoseyev, K. Batzner, R. Catherall, A.H.M. Evensen, D. ForkelWirth, O.C. Jonsson, E. Kugler, J. Lettry, V.I. Mishin, H.L. Ravn, G. Weyer, Nucl. Instr. Meth. Phys. Res. Sect. B 126 (1) (1997) 88.
[29] J.F. Ziegler, M.D. Ziegler, J.P. Biersack, Nucl. Instr. Meth. Phys. Res. Sect. B 268 (2010) 1818.
[30] U. Wahl, J.G. Correia, A. Czermak, S.G. Jahn, P. Jalocha, J.G. Marques, A. Rudge, F. Schopper, J.C. Soares, A. Vantomme, P. Weilhammer, ISOLDE Collaboration, Nucl. Instr. Meth. Phys. Res. Sect. A 524 (2004) 245.
[31] M.R. Silva, U. Wahl, J.G. Correia, L.M. Amorim, L.M.C. Pereira, Rev. Sci. Instrum. 84 (2013) 073506.
[32] U. Wahl, A. Vantomme, G. Langouche, J. Araujo, L. Peralta, J.G. Correia, ISOLDE Collaboration, J. Appl. Phys. 88 (2000) 1319.
[33] F. Takano, H. Ofuchi, J. Lee, K. Takita, H. Akinaga, Phys. B 376 (2006) 658.